Aging effect on the variation of Li-ion battery resistance as function of temperature and state of charge

Simone Barcellona[1], Silvia Colnago[1], Giovanni Dotelli[2], Saverio Latorrata[2], Luigi Piegari[1]

[1] Department of Electronics, Information and Bioengineering, Politecnico di Milano, Italy

[2] Department of Chemistry, Materials and Chemical Engineering "Giulio Natta", Politecnico di Milano, Italy

Abstract

Nowadays, lithium-ion batteries are widely employed in a lot of applications. Battery aging implies performance degradation of the battery itself. In particular, the battery aging causes capacity reduction and internal resistance increase. The capacity reduction mainly affects the energy that the battery can deliver in each cycle, while the increase of the internal resistance limits the power that the battery can instantaneously deliver. For this reason, the battery life is conventionally considered at its end when the capacity reaches 80% of the initial value or the resistance reaches 200% of the initial value. As is well known, the battery resistance changes with temperature and state of charge (SOC) and, even if this relationship was studied for new batteries, how this relationship changes with battery aging has not been studied yet. In this paper, the variation law of the internal resistance as a function of temperature and SOC at different aging conditions is analyzed. In particular, lithium battery cells were aged following a fixed protocol. During the aging process, electrochemical impedance spectroscopy was performed at different temperatures and SOCs to analyze the change of the battery impedance due to aging. By using the results of this experimental campaign, a mathematical model predicting how the internal battery resistance changes with temperature, SOC and aging is proposed. The effectiveness of the proposed model is validated by means of experimental tests and a chemical interpretation of phenomena is also provided.

I Introduction

Among the various rechargeable battery technologies, lithium-ion batteries (LiBs) are the most studied and widely employed because of their high power density, high energy density, low maintenance, and long lifespan [1,2]. For these reasons, LiBs are used in many different applications, which can be categorized into two main groups: stationary applications and mobile ones. The first category includes applications such as storage systems integrated with renewable energy sources and uninterruptable power systems. On the other hand, the applications in the second category range from small mobile applications (such as smartphones, notebooks, tablets…) to larger ones (such as electric vehicles and railway traction systems). In the latter, the energy and power are both of paramount importance. In fact, in traction applications, high energy is needed to guarantee a high range, while a high power ensures certain accelerations and performances of the vehicle. The energy of the battery is associated with its capacity, while the internal resistance is associated with the power that the battery can deliver. In recent years, the spread of electric vehicles has spurred an interest in research on

the state of health (SOH) of a battery, and therefore on the internal resistance increase and capacity fade. In this paper, the battery internal resistance increase will be analyzed and discussed.

A battery's internal resistance is composed of four contributions [3]. The first is the ohmic resistance (also called ac resistance), which represents the electronic and ionic resistance of the current collectors, terminals, electrodes, active material, electrolyte, and separator. The second is the resistance of the solid electrolyte interface (SEI) that starts to form in the first charge/discharge cycles and continues to increase over time during cycling and storage [4]. The third is the resistance related to the charge transfer process [5] associated with the chemical reactions. Finally, the last is the resistance related to the diffusion process [6] associated with the mass transport limitations of the electrodes and electrolytes [7]. This latter resistance is very difficult to estimate because it is related to high time constants.

In any case, a battery's internal resistance can be evaluated in different ways, which can be divided into two main groups: time-domain (dc) and frequency-domain (ac) estimations methods. The authors in [3] adopted the dc current pulse method, which injects a current pulse into a cell and measures the voltage change over different time intervals to find the different contributions of the internal resistance. Another possible technique is to calculate the heat loss during cell operation and use Joule's law to derive the resistance [8]. This second procedure has the same precision as the dc current pulse method but is more complicated and time-consuming. The voltage curve difference method is another possibility [9], where the cell is fully discharged at two different current rates, resulting in two voltage profiles. At a specific state of charge (SOC), the internal resistance is calculated as the difference in the voltage curves divided by the difference in the current rates. This method is very simple and rapid but it is very poor for modeling purposes [10]. The internal resistance can be evaluated by injecting a small alternating current with a constant frequency into the battery, which generates a small voltage [8]. The impedance is derived as the ratio between the variation in the voltage and the related variation in the current. The result of this procedure is dependent on the frequency of the signal. Different test equipment can give different results. Electrochemical impedance spectroscopy (EIS) allows the evaluation of the internal impedance values at different frequencies by injecting a small amplitude sinusoidal signal. This signal can be a current signal (galvanostatic electrochemical impedance spectroscopy) or a voltage signal (potentiostatic electrochemical impedance spectroscopy). This method gives detailed information on the cell behavior and, thanks to the utilization of small signals, provides results with no distortion. The drawback is that it requires expensive equipment. A detailed comparison of the methods is provided in [8].

As is widely known, a battery's internal resistance changes as a function of different factors such as the SOC and temperature. To build a model that predicts the battery behavior, it is important to know the relationship between battery resistance and operating conditions (i.e., temperature and SOC). In the literature, several studies can be found that analyzed how the SOC and temperature influence the battery internal resistance for different types of lithium-ion batteries.

The results of electrochemical spectroscopy performed at 50% of the SOC at many different temperatures were used in [11] to determine the internal resistance's variation law on the temperature in lithium-ion batteries. The authors in [12] performed EIS tests on two different types of lithium-ion batteries at certain SOC levels and several different temperatures and compared the results. In [13], the authors used the dc current pulse method to observe the internal resistance of a cylindrical lithium-ion battery at different SOCs and find the correlation between the internal resistance and the capacitance after some aging. In [10], the influence of the SOC on the internal resistance was analyzed: different cells were tested, and the resistances were evaluated with three different methods. The authors in [14] and [15] used the EIS to study the change in the impedance of a high-power battery with the variation of the temperature and SOC. A climatic chamber was used for the temperature variation. An evaluation of the internal resistance as a function of the SOC and temperature was performed in [3] using the dc pulse method. The influence of the amplitude and duration of the pulse on the resistance results was also investigated. All these studies considered the influences of the SOC and temperature on the internal resistance of lithium-ion batteries, but they did not analyze how the aging of the batteries changed the relationships between the internal resistance and the SOC and temperature. In fact, lithium-ion batteries are exposed to different degradation mechanisms according to the kind of chemistry used [16], [17], which limit their lifetime, performance, and efficiency. Nevertheless, it is well-known that such degradation mechanisms are caused by the storage conditions (calendar aging) and operating conditions (cycle aging) [18], [19]. The former mainly depend on the SOC and temperature as functions of time [20], [21]. The latter mainly depend on the total moved charge [22], current rate [21], and charging/discharging cut-off voltages [23], [24]. Nonetheless, under certain conditions, the current rate does not affect battery aging [25]. The calendar aging can be reduced by storing the battery at the best SOC and temperature values [26], [27]. The cycle aging can be reduced by changing the way a battery is subjected to loading conditions [28], i.e., by regulating its charge and discharge cycles, controlling the working temperature of the cells, or balancing the charge between different cells in a battery pack.

To extend the lifetime of a battery and optimize both the energy and power that can be exchanged, it is fundamental to build a system that controls the battery operating conditions. In particular, the long-term performance of LiBs has been proven to degrade rapidly if temperature is not kept in an optimal chemistry-related narrow range, therefore an effective cooling system is supposed to be desirable. This should guarantee, for both mobile and fixed applications, a protection against thermal runaway providing a balance between the highest possible discharge rate and the onset temperature for the runaway itself [29]. Another way to extend LiBs lifetime, improving at the same time performance, relies on materials development, particularly in terms of partial cation substitution and coating processes aiming to enhance the stability of the SEI interface and the overall structural integrity of electrodes [2]. A knowledge of the behavior of the battery and its careful prediction through an aging model is crucial for the proper control of the battery itself. Thus, the estimation and

analysis of internal battery parameters (internal resistance and capacity) as functions of aging are some of the most important keys to build more reliable tools.

In the literature, it is possible to find several aging models for both calendar aging and cycle aging as functions of different factors (such as the SOC, temperature, and current), and they are summarized and reviewed in [30]. Nevertheless, to build an aging model, it is necessary to choose a parameter that can estimate the aging of the cell. Based on the kind of degradation mechanism, the aging of batteries can lead to a reduction in their capacity (energy fade) or an increase in their internal resistance (power fade). For this reason, the SOH of a LiB can be related to one of these two indicators. In general, the end of life of a battery is considered to be when its capacity reaches 80% of its initial value or the internal resistance doubles [31].

It is possible to recognize that the internal parameters of LiBs directly depend on the same factors that age the battery. In fact, both the capacity and internal resistance mainly depend on the SOC, temperature, and current rate. This means that it is possible to estimate the SOH of a battery only if certain reference conditions of the SOC, temperature, and current are defined. On one hand, the literature contains much research on aging models, calculating the capacity fade and resistance increase due to the aging under certain conditions of SOC and temperature. Moreover, several papers can be found on the study of the law of variation of these parameters on the working conditions such as temperature and SOC. On the other hand, how these variation laws change with the battery aging seems to be lacking. In light of the above, in this paper, the authors want to fill this gap deeply analyzing how the variation law of the internal battery resistance as a function of the SOC and temperature changes with the cycle aging of the battery itself. This aspect is very important since, for many applications, the battery is considered at the end of its life if its internal resistance is doubled. Nevertheless, the internal resistance can be doubled at a certain temperature and SOC but it can result still lower than double in other temperature and SOC conditions. For this reason, it is very important to understand how the relationship, between battery resistance and operating conditions, changes with the battery aging. This aspect is studied in this paper by means of a large experimental campaign performed on LiB cells.

In the present work, the internal battery resistance estimation was conducted using the galvanostatic EIS in the frequency domain for different SOCs and temperatures. The battery cell was aged under fixed conditions for the SOC, temperature, and current rate. The internal resistance estimation was performed at the beginning of the life of the battery under test and after each aging cycle. In this way, the variation law of the internal resistance as function of the SOC and temperature was estimated in different aging conditions.

II. Battery Model

Several electric battery models can be found in the literature, with different approaches and levels of detail. Equivalent circuit models are the most commonly used because they assure a good trade-off between accuracy and complexity [30].

One of the most exhaustive circuit models is reported in [32] and presented in Figure I(a). It consists of an ideal voltage source with a series resistance, two parallel R/CPE branches (consisting of a resistor in parallel to a constant phase element), and the so-called Warburg impedance. The ideal voltage source (V_{OC}) represents the voltage of the cell when no current flows. This parameter depends on the type of battery, SOC, temperature, and SOH. The resistances reported in Figure I(a) are related to the four different contributions, as discussed in the introduction. In particular, R_s is the pure ohmic resistance (ac resistance), R_{SEI} is the resistance of the SEI, and R_{ct} is the resistance related to the charge transfer effect. The resistance related to the diffusion process is considered in Warburg element Z_W. CPE_{SEI} represents the capacity behavior of the SEI, and CPE_d is the double layer capacitance between each electrode and the electrolyte. All these parameters in the frequency domain led to the Nyquist plot reported in Figure I(b). In particular, the impedances of the SEI and charge transfer are related to the first two semicircles in the plane, while the diffusion process is the last part of the spectrum. According to Figure 1(a), from a circuital point of view, the low frequency resistance is the sum of all the above-mentioned resistance terms, as expressed in (1). To find this, we chose to use the galvanostatic EIS method running from 10 kHz to 100 mHz to obtain the different terms. To estimate even the diffusion resistance term, which is related to the diffusion process (Warburg impedance), the EIS tests should be conducted with very low frequencies (theoretically down to zero). This is a very difficult task because at low frequencies the EIS tests become very long and unstable. Moreover, the sum of the pure ohmic resistance and the SEI and charge transfer ones can be taken as the low frequency resistance because their time constants are in the range of interest for describing the power capability of the battery [33]. Therefore, the low frequency resistance is defined as follows:

$$R_{LF} = R_s + R_{SEI} + R_{ct}. \tag{1}$$

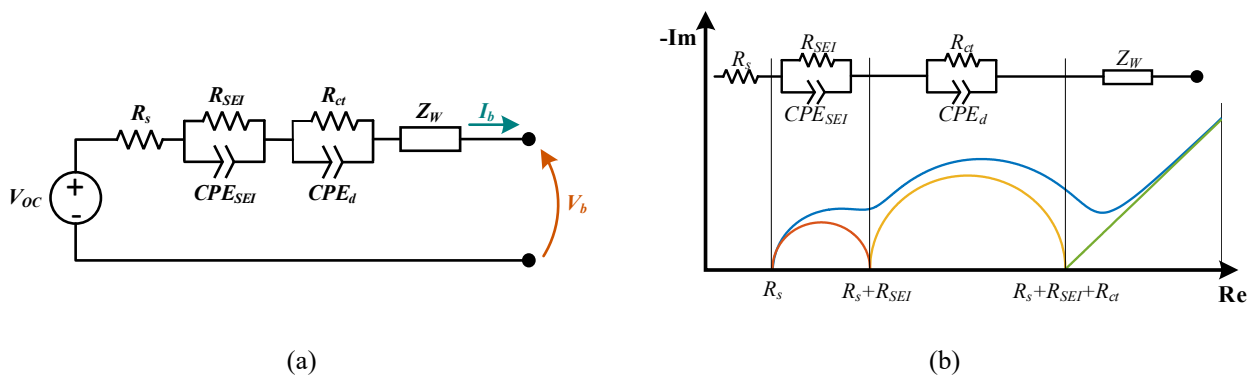(a)   (b)

Figure 1 a) Equivalent circuit model of lithium-ion battery and b) Nyquist plot of lithium-ion battery

In the present work, we are interested in calculating the internal resistances as an indicator of the SOH, analyzing how the variation of this parameter on the SOC and temperature changes with the aging. The latter is quantified using the total moved charge (expressed in Ah) exchanged with the battery, and thus defined as follows:

$$Q = \frac{1}{3600} \int_0^t |I_b| d\tau. \tag{2}$$

However, the capacity fade in per unit, calculated at 25 °C, is reported in Figure 2, to give a better understanding of the aging of the analyzed battery for any moved charge.
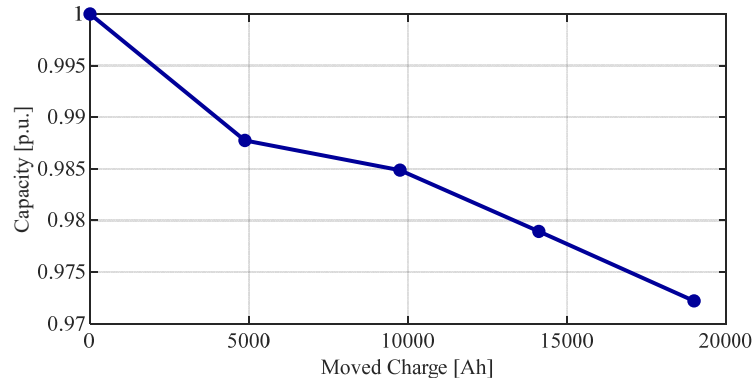

Figure 2 Per unit capacity fade

III. Aging procedure

Cell under study

The battery cell under study is a lithium cobalt oxide cell 8773160K manufactured by General Electronics Battery Co. Ltd. The main parameters of the cell are summarized in Table 1.

Table 1 Battery Cell Specifications

Parameter	Value	Units
Rated Capacity	10	Ah
Rated Voltage	3.7	V
Charge Cut-off Voltage	4.2	V
Discharge Cut-off Voltage	2.75	V
Maximum Continuous Discharge Current	100 (10C)	A
Maximum Peak Discharge Current	150 (15C)	A
Weight	228	g

Test setup

Tests were performed using a 100 A booster (VMP3B-100) from Biologic Science Instruments, connected to a potentiostat (SP-150) controlled by a PC with EC-LAB software via an Ethernet cable. An overview of the test setup is depicted in Figure 3.
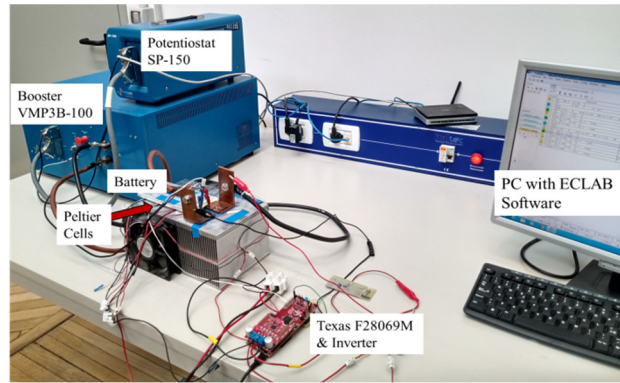
Figure 3 Test setup overview

To control and maintain a constant battery temperature during the tests, three Peltier cells were connected in series and placed under the battery itself. It is worth noting that the climatic chamber maintains a constant room temperature, but not a constant battery temperature under different current rates, whereas controlling the Peltier cells made it possible to directly control the battery temperature. The control of the Peltier cells was performed through an F28069M microcontroller by Texas instruments connected to a DRV8323RX inverter. A full-bridge converter was used, and the Peltier cells were connected between two legs. A temperature probe was placed on the battery. The microcontroller read the temperature measured by the probe and compared it with the reference temperature. The error was input to a proportional-integral (PI) controller, which output a pulse width modulation (PWM) control signal for the inverter. The temperature control scheme is reported in Figure 4.
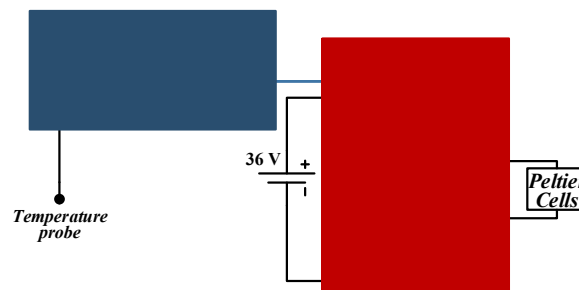

Figure 4 Temperature control scheme

Test procedure

The test procedure consisted of two steps: the resistance measurement and aging cycle. The former was performed at the beginning of the test to measure the initial battery resistances, and after each aging cycle phase to evaluate the resistance increase.

Internal resistances measurement

The cell resistances were tested at eight different reference temperatures: 20 °C, 22.5 °C, 25 °C, 27.5 °C, 30 °C, 33.5 °C, 38 °C, and 46 °C. In practice, since the system controlling the temperature was not able to exactly track the reference temperature, the measurements were performed in a range of 2 °C around the reference values. For each temperature, the

internal resistances were evaluated at five different SOC levels: battery fully charged (i.e., SOC = 100%), 75%, 50%, 25%, and battery fully discharged (i.e., SOC = 0%).

The test procedure was as follows. The cell was charged to 100% of the SOC with a constant current-constant voltage (CCCV) charging protocol: the cell was charged with 1C until reaching the charge cut-off voltage, then a constant voltage of 4.2 V was applied until the current of the cell decayed to 0.01C. When the charging was completed, the cell was left to rest for 1 hour. After 1 hour of relaxation time, the galvanic EIS was performed to evaluate the resistance. Afterward, the cell was discharged to 75% of the SOC. At this new SOC level, after 1 hour of relaxation time, another galvanic EIS was performed. The same procedure was repeated, discharging the cell by 25% of the SOC at a time until 0% SOC. After evaluating the resistances of the fully discharged battery, the cell was charged to 100% of the SOC, and the same procedure was repeated for the other temperatures.

Aging cycles

The resistances were measured after each aging cycle obtained by moving 5000 Ah. The aging cycles were performed at a constant reference temperature of 30 °C. A charge and discharge current of 5C was chosen to speed up the test, because, as reported in [25], the current rate under these conditions does not influence the aging. Because the capacitance of the cell decreases with aging, after moving 10000 Ah, the current was decreased to 4C to avoid the high-frequency aging effect [34]. The charge and discharge cycles were limited by two boundaries: the SOC was limited to 20–80%, and the voltage was limited to 3.45–4.05 V. It is worth noting that if the voltage limits are reached before the SOC boundaries, the charge moved in one cycle is less than 6 Ah. However, the results of [22] show that the aging of the battery does not depend on the cycle shape, but only on the moved charge.

IV. Analysis of Results

The ac and the low frequency resistance were calculated from the EIS performed in the above-mentioned conditions. Zview® software (Scribner Associates) has been adopted to fit the EIS experimental data by using the equivalent circuit shown in Figure 1(a) in order to determine the different electrochemical parameters and contributions [35]. Considering the adopted model, the ohmic resistance is the high frequency intersection of the spectrum with the real axis. In such model, it is in series with two parallel resistance/constant phase element circuits, R_{SEI}/CPE_{SEI} and R_{ct}/CPE_d, modelling, at decreasing frequency (namely, SEI's contribution is visible at a relatively higher frequency) the activation polarization due to the passivation layer related to the SEI and the charge transfer of the double layer at electrodes surface, respectively. The diameter of the semicircles originating from spectra deconvolution (Figure 5) represents the inner resistance of the SEI and the charge transfer resistance. Constant phase elements (CPE) were used instead of pure capacitances to account for the capacitive losses that generally occur in porous electrodes. The Warburg element Z_W models the diffusive behavior within the electrolyte at low frequency and can be considered as a mass transfer resistance. Ideally, the real part of its

impedance equals the imaginary part, so it is represented by a 45° line following the charge transfer semicircle; it deviates from such ideal line depending on the specific operating conditions employed.
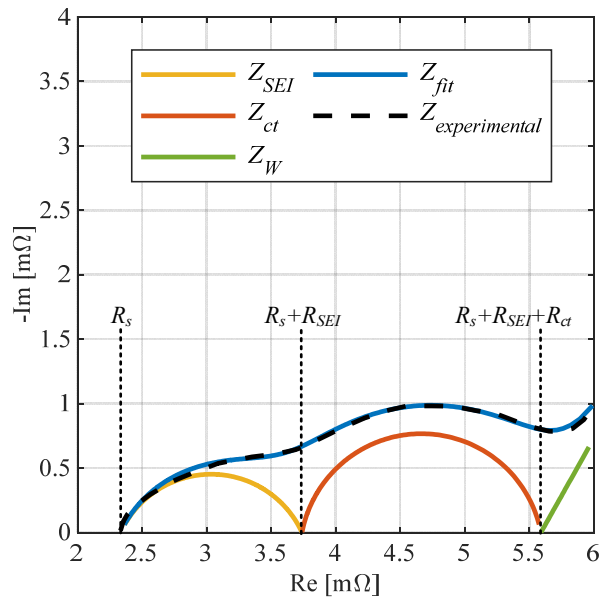

Figure 5 Nyquist plot at 30 °C and SOC 0% after 5000 Ah

For each tested SOC and aging condition, the experimental values of the ac and low frequency internal resistances as a function of the temperature, together with their fitting functions, are shown in Figure 6 and Figure 7 respectively.
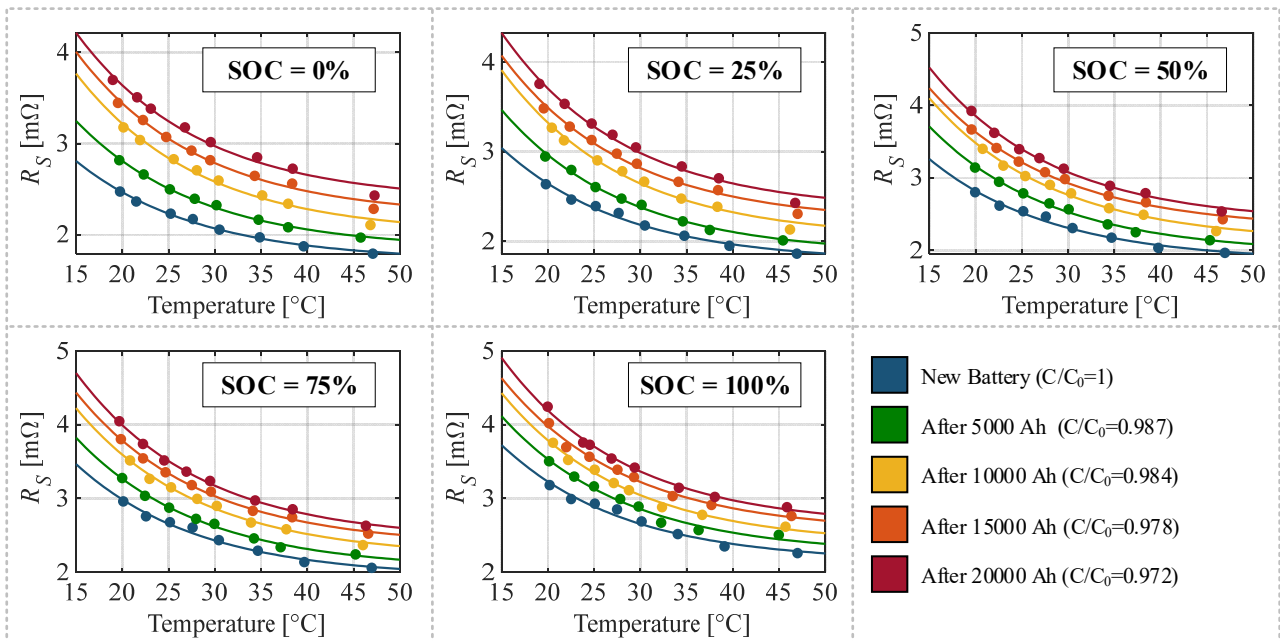

Figure 6 ac resistance at different temperature and aging conditions: experimental data (marked points) and fitting (continuous lines)
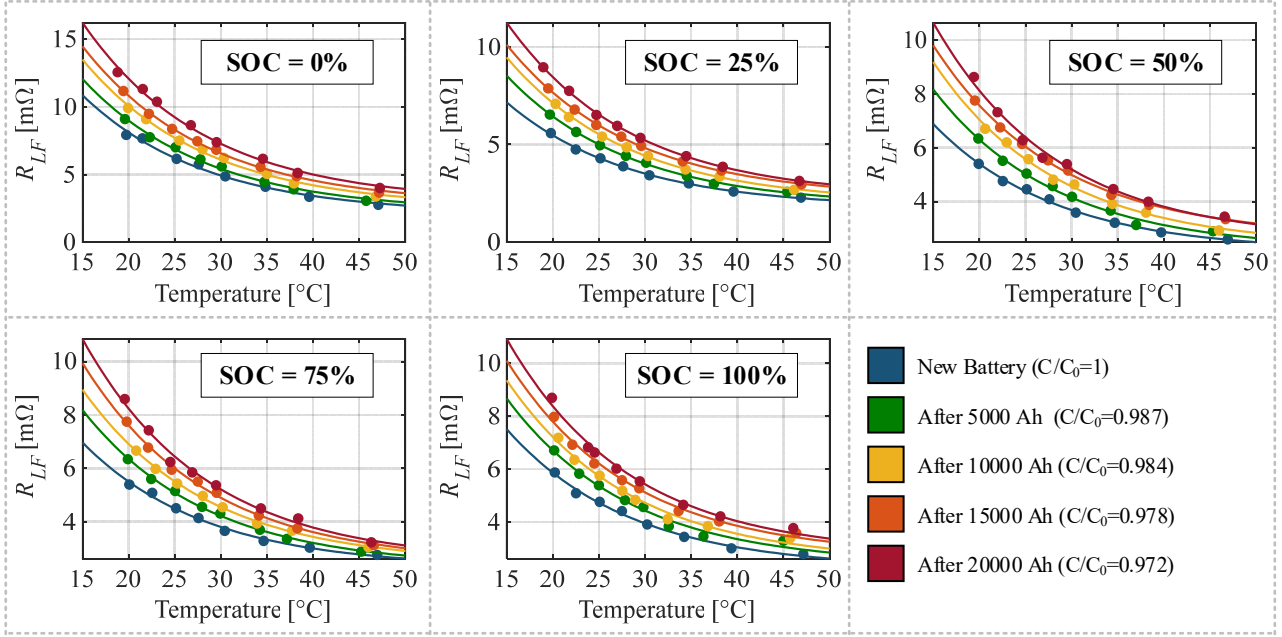
Figure 7 Low frequency resistance at different temperature and aging conditions: experimental data (marked points) and fitting (continuous lines)

It can be noted that, for both ac and low frequency resistances in all the cases, the resistance decreased exponentially with the temperature. Therefore, the experimental data were fitted with the following exponential function:

$$R(T) = ae^{-bT} + c \, , \tag{3}$$

where T is the temperature, and a, b, and c are the fitting coefficients. Through this fitting, coefficient b remained fairly constant for each aging condition and SOC. Consequently, the fitting of the experimental data was performed again with coefficient b constant at 0.075.

For both ac and low frequency resistances and for all the tested SOCs, the coefficients a and c increase with the moved charge. The coefficients were, in turn, fitted with linear functions as follows:

$$\begin{aligned} a(Q,SOC) &= m_a(SOC)Q + q_a(SOC) \\ c(Q,SOC) &= m_c(SOC)Q + q_c(SOC) \end{aligned} \, , \tag{4}$$

where Q is the moved charge, and m_a, q_a, m_c, and q_c are the parameters of the fitting functions of the coefficients a and c. Results of coefficients and their fitting functions are reported in Figure 8 and Figure 9 for ac and low frequency resistances, respectively.
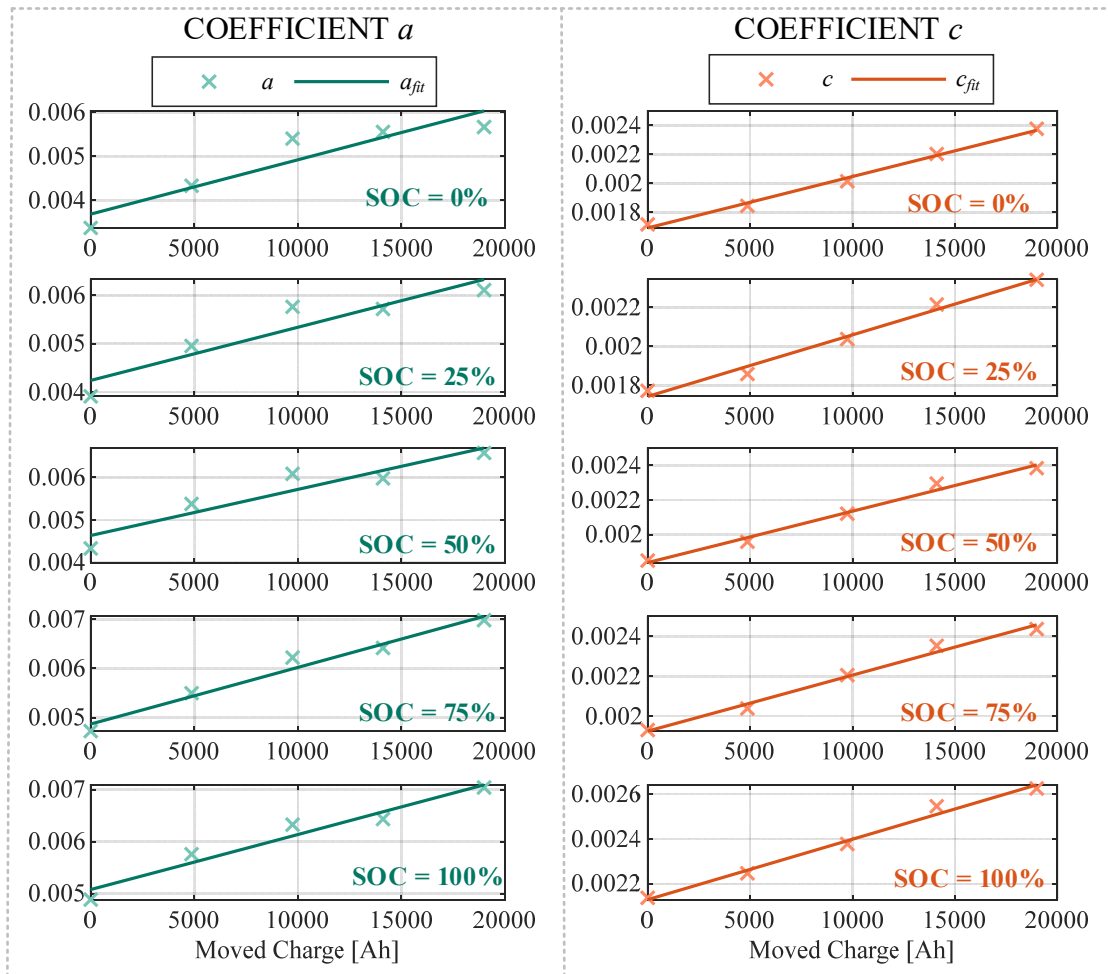
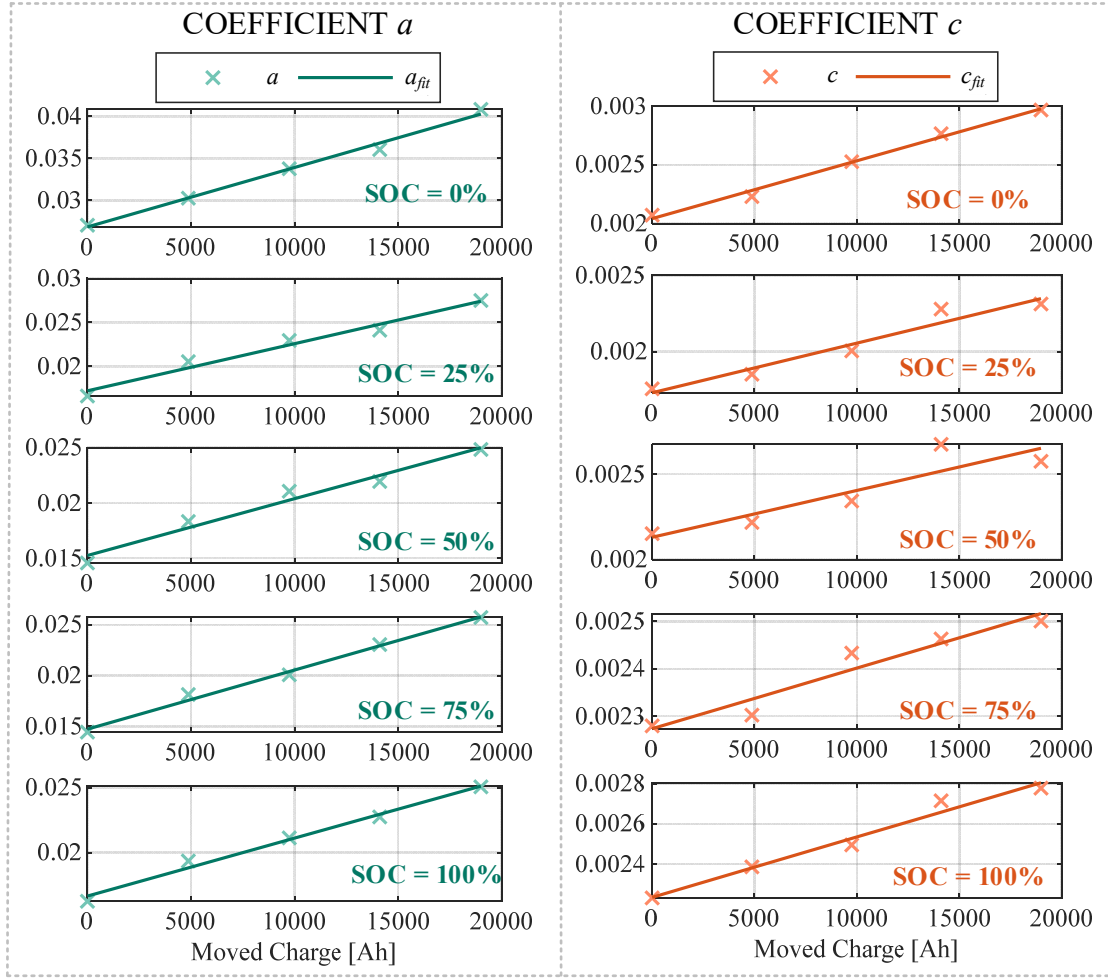Figure 8 Coefficients *a* and *c* for ac resistance with respect to the moved charge

Figure 9 Coefficients *a* and *c* for low frequency resistance with respect to the moved charge

Table *2* lists the parameters of the lines reported in Figure 8 and Figure 9.

Table 2 Coefficients for *a* and *c*

			State of Charge				
			0%	25%	50%	75%	100%
R_s	a	m_a	$1.238*10^{-7}$	$1.102*10^{-7}$	$1.084*10^{-7}$	$1.153*10^{-7}$	$1.059*10^{-7}$
		q_a	0.0037	0.0042	0.0046	0.0049	0.0051
	c	m_c	$3.549*10^{-8}$	$3.16*10^{-8}$	$2.964*10^{-8}$	$2.808*10^{-8}$	$2.684*10^{-8}$
		q_c	0.0017	0.0017	0.0018	0.0019	0.0021
R_{LF}	a	m_a	$7.058*10^{-7}$	$5.375*10^{-7}$	$5.143*10^{-7}$	$5.814*10^{-7}$	$4.462*10^{-7}$
		q_a	0.027	0.0172	0.0152	0.0147	0.0167
	c	m_c	$4.92*10^{-8}$	$3.233*10^{-8}$	$2.744*10^{-8}$	$1.276*10^{-8}$	$3.01*10^{-8}$
		q_c	0.002	0.0017	0.0021	0.0023	0.0022

Finally, an aging model can be developed, in which the variation law of the internal resistances with the temperature is calculated as in (3), in which *a* and *c* are calculated according to (4). Figure 10 and Figure 11 report the experimental

data and the results of the model for ac and low frequency resistances respectively, in all tested SOCs and aging conditions. It is worth noting that the model well matched the experimental data.
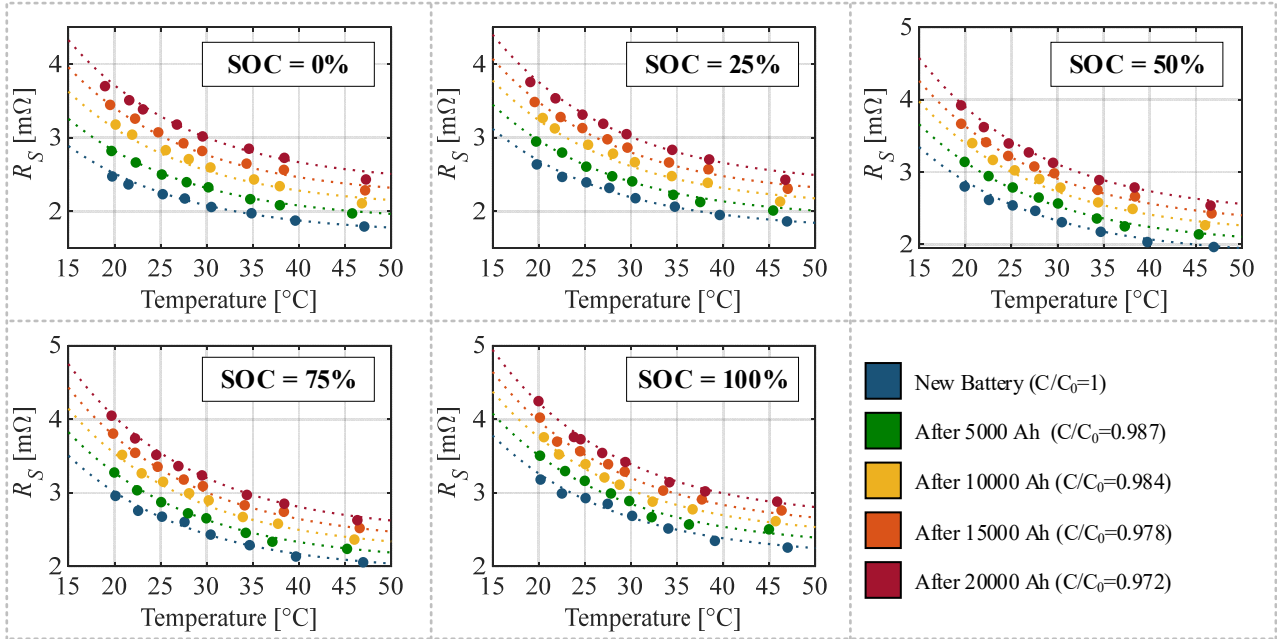

Figure 10 Variation of ac resistance as function of temperature: experimental data (marked points) and model (dotted lines)
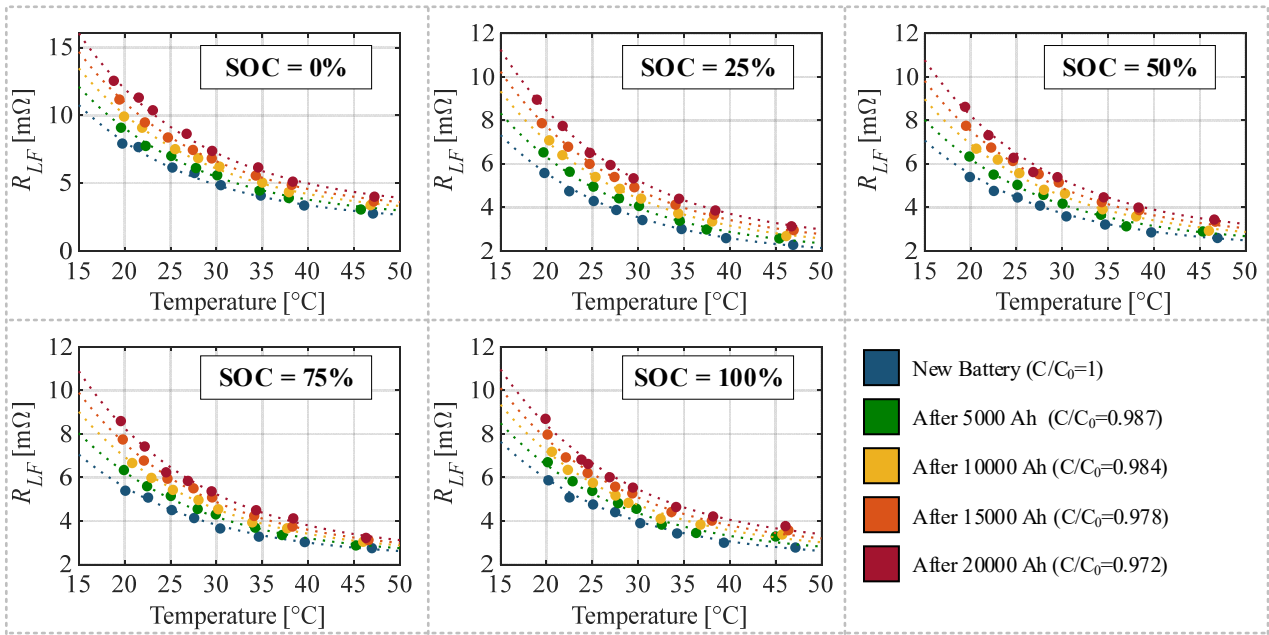

Figure 11 Variation of low frequency resistance as function of temperature: experimental data (marked points) and model (dotted lines)

For defined conditions of SOC, it is interesting to rearrange (3) to show the link between the actual internal resistance and the initial value in terms of aging.

$$R(T,Q,SOC) = k(Q,SOC) \cdot R(T,0,SOC) + h(Q,SOC) \tag{5}$$

Taking into account (3) and (4) in (5), parameters k and h result in the following:

$$k(Q,SOC) = \frac{a(Q,SOC)}{a(0,SOC)} = 1 + \frac{m_a(SOC)}{q_a(SOC)}Q$$

$$h(Q,SOC) = c(Q,SOC) - k(Q,SOC) \cdot c(0,SOC) = \frac{m_c(SOC)q_a(SOC) - m_a(SOC)q_c(SOC)}{q_a(SOC)}Q.$$

(6)

In this way, it is possible to highlight how, for a given SOC, the variation law of the resistance on the temperature changes as a function of the moved charge, i.e., the aging. It is worth noting that gain term k causes the resistance to increase by the same percentage for all the temperatures. On the other hand, offset term h increases all the resistances by the same absolute value. According to the results, the internal resistance increase, as a function of the aging conditions, is not the same in percentage terms at all the temperatures and SOC levels, unlike what was highlighted in [33] for lithium nickel manganese cobalt oxide batteries. This is the main outcome of the present work. In particular, as one can infer from the slope of the curves in Figure 12 and Figure 13, for all the SOC levels, the per-unit increase in the ac and low frequency resistances is higher for a lower temperature, i.e. the slope of the curves is higher for lower temperatures. For example, considering the case of the low frequency resistance at 50% of the SOC, the experimental data showed that the resistance of the new battery at 20 °C was 5.40 mΩ, and at 46 °C it was 2.59 mΩ. Using the model developed in this study, these two resistances could be estimated to be 5.53 mΩ at 20 °C and 2.59 mΩ at 46 °C (with an error lower than 2.6%). The resistance measured after 20000 Ah at 46 °C was 3.44 mΩ, which represented an increase of 33% with respect to the new battery at the same temperature, while the one measured at 20 °C was 8.62 mΩ, which represented an increase of 59%. The model developed in this study allows a precise prediction of these resistances, with results of 8.23 mΩ and 3.41 mΩ at 20 °C and 46 °C, respectively (with an error lower than 4.5%). If we had considered the increase in the low frequency resistance to be the same at all the temperatures and the percentage of increase in the resistance to be that at 46 °C, the resistance at 20 °C after 20000 Ah would have been estimated to be 7.12 mΩ instead of 8.62 mΩ (with an error of 17.4%). Therefore, this assumption would have led to an underestimation of the low frequency resistance, which could lead to the battery being used even if it had already reached the end of its life. This condition could lead to a lack of power and safety issues for several applications.
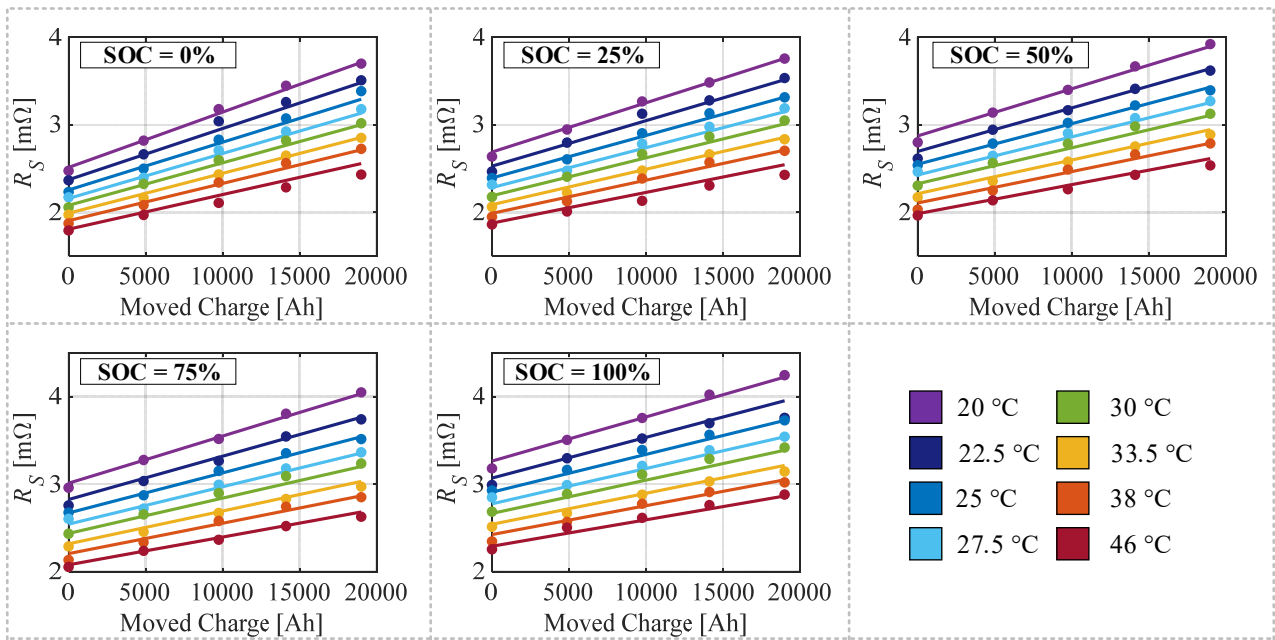
Figure 12 Variation of ac resistance with the moved charge: experimental data (marked points) and model (continuous lines)
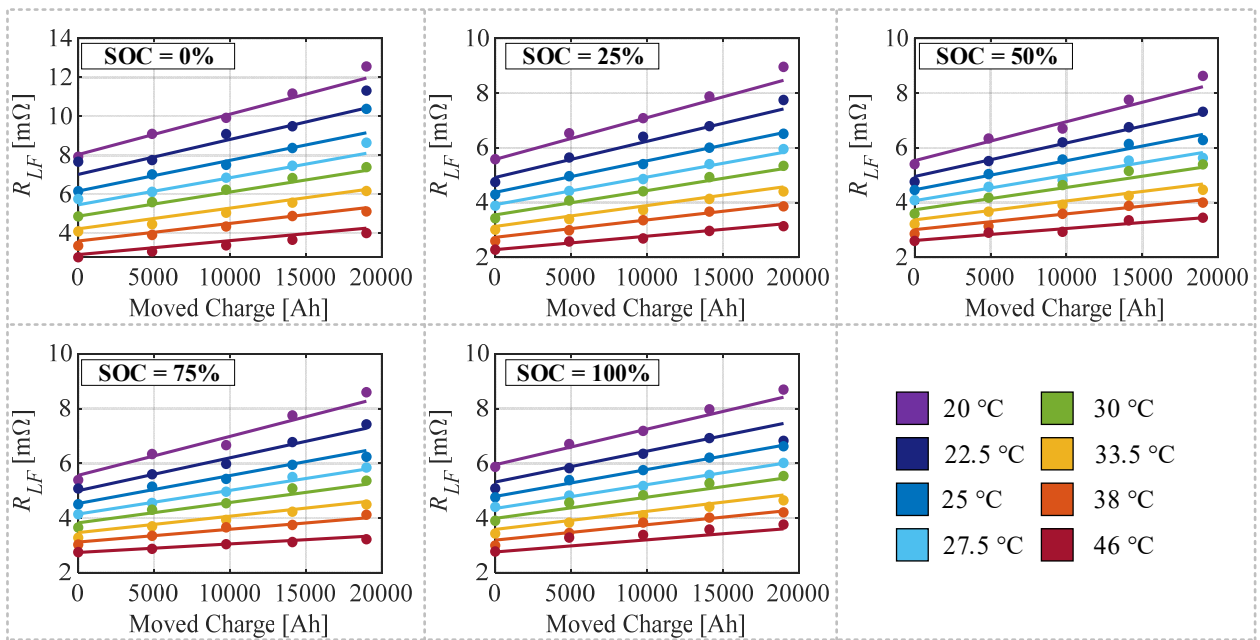

Figure 13 Variation of low frequency resistance with the moved charge: experimental data (marked points) and model (continuous lines)

Figure 14 and Figure 15 report the relative error of the value estimated with the proposed model with respect to the experimental value, for ac and low frequency resistance respectively. It is worth noting that the error is below 5% for the ac resistance and below 8% for the low frequency resistance. As is shown in the figures, the error in estimating the low frequency resistance is higher than the error in estimating the ac resistance. In any case, except from few points, the error is always lower than 5% that is a very good result taking into account the simplicity of the model that is used to estimate the battery cell resistance in a wide range of SOC, temperature and aging.
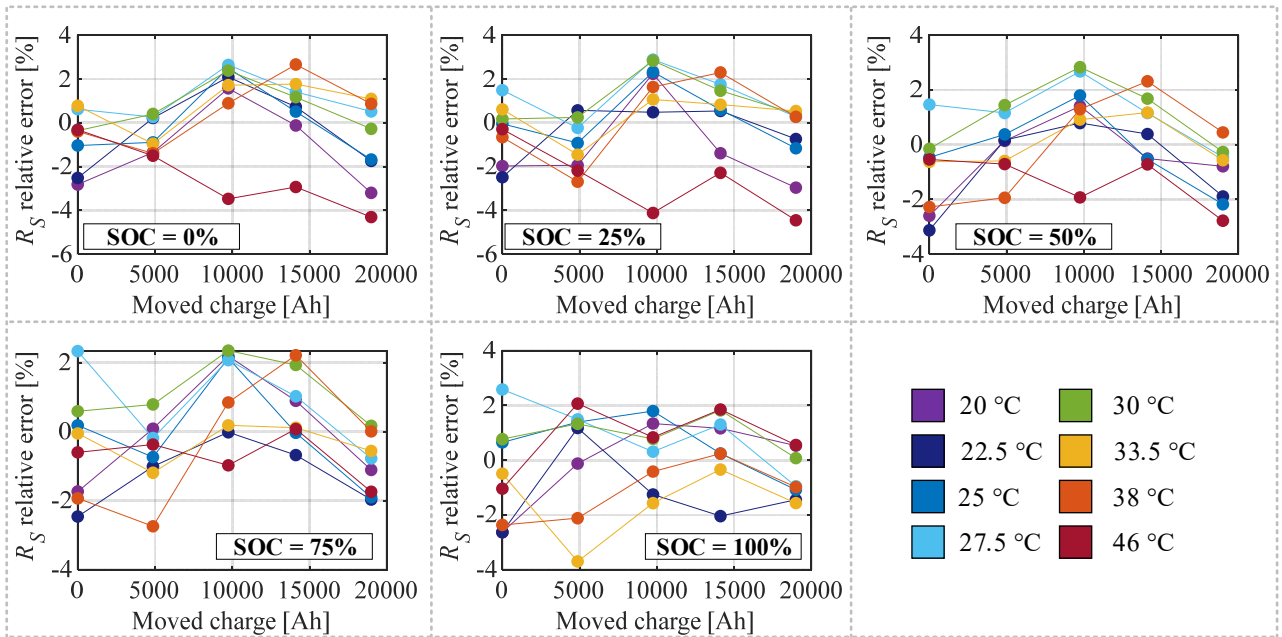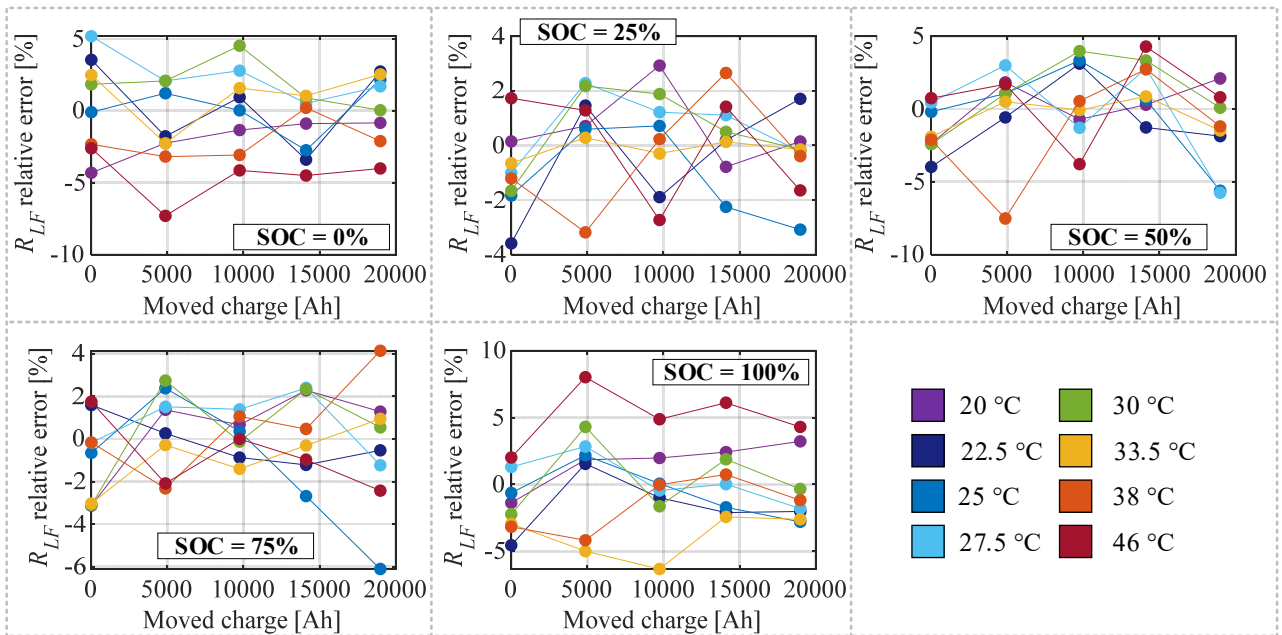
Figure 14 ac resistance relative error

Figure 15 low frequency resistance relative error

V. Chemical analysis

The observed increase in resistance should be ascribed to the variation of the electrolyte, interface, and charge transfer resistance, along with the double layer capacitance during the battery cycling [36].

The electrode surface area loss could be considered a crucial factor affecting the resistance. This is detrimental for both anodes and cathodes hosting Li$^+$ ions during the charge/recharge process, but it can be more critical for the

carbonaceous-based materials used for the anodic compartment because they are more prone to exfoliation (especially if graphitic carbon is employed), and their nanoparticles can easily coalesce [37]. Such surface area loss is supposed to worsen the charge transfer because the available sites for Li-ion adsorption/desorption may be limited, and the interconnections between conductive particles are reduced, affecting the efficacy and velocity of the charge paths. Moreover, the electrode surface degradation may also give rise to an increase in material roughness, especially for the graphite-based anode, which reduces the effectiveness of the contact between the electrode and electrolyte, negatively affecting the overall ohmic resistance [36]. The ceramic cathodic material is instead degraded by cracks and defects in the constituting particles, as well as microstructural changes induced by the continuous formation and breakage of chemical bonds during the electrochemical process [37].

Upon increasing the battery cycling, the growth of the electrode–electrolyte interface layer may also play a role in the overall resistance change. The kinetic aspects of the redox process are also influenced, and the exchange current density decreases accordingly [36].

A further drawback is related to the behavior of the cathodic redox couple, Co^{3+}/Co^{4+}. During the charge phase, Co^{3+} is oxidized to Co^{4+}, which can quickly react with the electrolyte and dissolve in it. This may damage the SEI on the carbon-based anode, leading to larger Li metallic deposits and consequently to a higher interface impedance [38].

The fact that the change in resistance is restrained at higher temperatures may be due to the higher mobility of the charges (Arrhenius-type dependence on temperature), which leads to a relatively more efficient charge transfer compared to what takes place at lower temperatures [33]. The effects of the electrode degradation in terms of the increase in roughness and loss of surface area are supposed to be crucial in determining a worse charge transfer at any temperature. However, at higher temperatures, such a drawback may be counterbalanced by the better mobility, which in turn can positively affect the change in the overall resistance.

VI. Conclusions

The increasing of internal battery resistance with battery aging is one of the critical aspects limiting the lifetime of batteries. It is well known that battery internal resistance changes with temperature and SOC. Nevertheless, it was never studied how the battery aging influences the relationship between internal resistance and operating conditions (i.e., temperature and SOC). In this study, an analysis of how the variation law of the battery internal resistance as function of the SOC and temperature changes with battery aging, was performed. The ac and low frequency battery resistances were estimated by using the galvanostatic EIS in the frequency domain for different SOCs, temperatures, and aging conditions. The aging cycles were performed at constant temperatures and current rates.

A mathematical model of the variation law of resistances as function of the SOC and temperature was proposed and validated. The proposed model showed a good match with the experimental data. In particular, the proposed model is

capable of predicting the ac and low frequency resistances of the battery in a very wide range of SOC, temperature and aging condition with a good accuracy (the relative error is always lower than 5% for the estimation of the ac resistance and lower than 8% for the estimation of the low frequency resistance)

From the results, it was possible to recognize that both the ac and low frequency resistances increase with the battery aging but showing different percentage variations for different temperatures and SOC levels. In particular, the resistance increasing was higher at lower temperatures. From the chemical analysis, it was possible to suppose that at higher temperatures, the better ion mobility counterbalanced the electrode degradation, positively affecting the resistance increase. For this reason, the increase of the battery internal resistance represents a more significant limitation for batteries working at lower temperatures. Finally, it is worth noting that the internal resistance increasing can be significant (up to 68%) even if the capacity fade is still limited (lower than 3%) as shown in the presented results.

References

[1]   S. Pelletier, O. Jabali, G. Laporte, M. Veneroni, Battery degradation and behaviour for electric vehicles: Review and numerical analyses of several models, Transportation Research Part B: Methodological. 103 (2017) 158–187. https://doi.org/10.1016/j.trb.2017.01.020.

[2]   A.M. Divakaran, M. Minakshi, P.A. Bahri, S. Paul, P. Kumari, A.M. Divakaran, K.N. Manjunatha, Rational design on materials for developing next generation lithium-ion secondary battery, Progress in Solid State Chemistry. 62 (2021) 100298. https://doi.org/10.1016/j.progsolidstchem.2020.100298.

[3]   B. V Ratnakumar, M.C. Smart, L.D. Whitcanack, R.C. Ewell, The impedance characteristics of Mars Exploration Rover Li-ion batteries, Journal of Power Sources. 159 (2006) 1428–1439. https://doi.org/https://doi.org/10.1016/j.jpowsour.2005.11.085.

[4]   V.A. Agubra, J.W. Fergus, The formation and stability of the solid electrolyte interface on the graphite anode, Journal of Power Sources. 268 (2014) 153–162. https://doi.org/10.1016/j.jpowsour.2014.06.024.

[5]   J. Li, E. Murphy, J. Winnick, P.. Kohl, Studies on the cycle life of commercial lithium ion batteries during rapid charge–discharge cycling, Journal of Power Sources. 102 (2001) 294–301. https://doi.org/10.1016/S0378-7753(01)00821-7.

[6]   G. Ning, B. Haran, B.N. Popov, Capacity fade study of lithium-ion batteries cycled at high discharge rates, Journal of Power Sources. 117 (2003) 160–169. https://doi.org/10.1016/S0378-7753(03)00029-6.

[7]   T.B. Reddy, D. Linden, Linden's handbook of batteries, McGraw-Hill, New York, NY, 2011.

[8]   H.-G. Schweiger, O. Obeidi, O. Komesker, A. Raschke, M. Schiemann, C. Zehner, M. Gehnen, M. Keller, P. Birke, Comparison of Several Methods for Determining the Internal Resistance of Lithium Ion Cells, Sensors. 10 (2010) 5604–5625. https://doi.org/10.3390/s100605604.

[9]   M. Dubarry, C. Truchot, M. Cugnet, B.Y. Liaw, K. Gering, S. Sazhin, D. Jamison, C. Michelbacher, Evaluation of commercial lithium-ion cells based on composite positive electrode for plug-in hybrid electric vehicle applications. Part I: Initial characterizations, Journal of Power Sources. 196 (2011) 10328–10335. https://doi.org/https://doi.org/10.1016/j.jpowsour.2011.08.077.

[10]   D. Anseán, V.M. García, M. González, J.C. Viera, C. Blanco, J.L. Antuña, DC internal resistance during charge: Analysis and study on LiFePO<inf>4</inf> batteries, in: 2013 World Electric Vehicle Symposium and Exhibition (EVS27), 2013: pp. 1–11. https://doi.org/10.1109/EVS.2013.6914746.

[11]   T. Momma, M. Matsunaga, D. Mukoyama, T. Osaka, Ac impedance analysis of lithium ion battery under temperature control, Journal of Power Sources. 216 (2012) 304–307. https://doi.org/https://doi.org/10.1016/j.jpowsour.2012.05.095.

[12]   S. Hossain, X. Kang, S. Shrestha, Effects of Temperature on Internal Resistances of Lithium-Ion Batteries, Journal of Energy Resources Technology. 137 (2015) 31901. https://doi.org/10.1115/1.4028698.

[13]   Y. Bao, W. Dong, D. Wang, Online Internal Resistance Measurement Application in Lithium Ion Battery Capacity and State of Charge Estimation, Energies . 11 (2018). https://doi.org/10.3390/en11051073.

[14]   D. Andre, M. Meiler, K. Steiner, C. Wimmer, T. Soczka-Guth, D.U. Sauer, Characterization of high-power lithium-ion batteries by electrochemical impedance spectroscopy. I. Experimental investigation, Journal of Power Sources. 196 (2011) 5334–5341. https://doi.org/https://doi.org/10.1016/j.jpowsour.2010.12.102.

[15]   J. Gomez, R. Nelson, E.E. Kalu, M.H. Weatherspoon, J.P. Zheng, Equivalent circuit model parameters of a high-power Li-ion battery: Thermal and state of charge effects, Journal of Power Sources. 196 (2011) 4826–4831. https://doi.org/https://doi.org/10.1016/j.jpowsour.2010.12.107.

[16]   X. Han, M. Ouyang, L. Lu, J. Li, Y. Zheng, Z. Li, A comparative study of commercial lithium ion battery cycle life in electrical vehicle: Aging mechanism identification, Journal of Power Sources. 251 (2014) 38–54. https://doi.org/https://doi.org/10.1016/j.jpowsour.2013.11.029.

[17]   X. Han, L. Lu, Y. Zheng, X. Feng, Z. Li, L. Jianqiu, M. Ouyang, A review on the key issues of the lithium ion battery degradation among the whole life cycle, ETransportation. 1 (2019) 100005. https://doi.org/10.1016/j.etran.2019.100005.

[18]   I. Bloom, B.W. Cole, J.J. Sohn, S.A. Jones, E.G. Polzin, V.S. Battaglia, G.L. Henriksen, C. Motloch, R. Richardson, T. Unkelhaeuser, D. Ingersoll, H.L. Case, An accelerated calendar and cycle life study of Li-ion cells, Journal of Power Sources. 101 (2001) 238–247. https://doi.org/https://doi.org/10.1016/S0378-7753(01)00783-2.

[19]   R.B. Wright, C.G. Motloch, J.R. Belt, J.P. Christophersen, C.D. Ho, R.A. Richardson, I. Bloom, S.A. Jones, V.S. Battaglia, G.L. Henriksen, T. Unkelhaeuser, D. Ingersoll, H.L. Case, S.A. Rogers, R.A. Sutula, Calendar- and cycle-life studies of advanced technology development program generation 1 lithium-ion batteries, Journal of Power Sources. 110 (2002) 445–470. https://doi.org/https://doi.org/10.1016/S0378-7753(02)00210-0.

[20]   K. Nunotani, F. Yoshida, Y. Kamiya, Y. Daisho, K. Abe, M. Kono, H. Matsuo, Development and performance evaluation of lithium iron phosphate battery with superior rapid charging performance-Second report: Evaluation of battery capacity loss characteristics, in: 2011 IEEE Vehicle Power and Propulsion Conference, IEEE, 2011: pp. 1–4. https://doi.org/10.1109/VPPC.2011.6042998.

[21]   S.S. Choi, H.S. Lim, Factors that affect cycle-life and possible degradation mechanisms of a Li-ion cell based on LiCoO2, Journal of Power

Sources. 111 (2002) 130–136. https://doi.org/10.1016/S0378-7753(02)00305-1.

[22]   S. Barcellona, M. Brenna, F. Foiadelli, M. Longo, L. Piegari, Analysis of Ageing Effect on Li-Polymer Batteries, The Scientific World Journal. 2015 (2015) 1–8. https://doi.org/10.1155/2015/979321.

[23]   K. Asakura, M. Shimomura, T. Shodai, Study of life evaluation methods for Li-ion batteries for backup applications, Journal of Power Sources. 119–121 (2003) 902–905. https://doi.org/10.1016/S0378-7753(03)00208-8.

[24]   H. Gong, Y. Yu, T. Li, T. Mei, Z. Xing, Y. Zhu, Y. Qian, X. Shen, Solvothermal synthesis of LiFePO4/C nanopolyhedrons and microellipsoids and their performance in lithium-ion batteries, Materials Letters. 66 (2012) 374–376. https://doi.org/10.1016/j.matlet.2011.08.093.

[25]   S. Barcellona, L. Piegari, Effect of current on cycle aging of lithium ion batteries, Journal of Energy Storage. 29 (2020) 101310. https://doi.org/10.1016/j.est.2020.101310.

[26]   P. Keil, S.F. Schuster, J. Wilhelm, J. Travi, A. Hauser, R.C. Karl, A. Jossen, Calendar Aging of Lithium-Ion Batteries, Journal of The Electrochemical Society. 163 (2016) A1872–A1880. https://doi.org/10.1149/2.0411609jes.

[27]   M. Schimpe, M.E. von Kuepach, M. Naumann, H.C. Hesse, K. Smith, A. Jossen, Comprehensive Modeling of Temperature-Dependent Degradation Mechanisms in Lithium Iron Phosphate Batteries, Journal of The Electrochemical Society. 165 (2018) A181–A193. https://doi.org/10.1149/2.1181714jes.

[28]   B.P. Divakar, K.W.E. Cheng, H.J. Wu, J. Xu, H.B. Ma, W. Ting, K. Ding, W.F. Choi, B.F. Huang, C.H. Leung, Battery management system and control strategy for hybrid and electric vehicle, in: 2009 3rd International Conference on Power Electronics Systems and Applications (PESA), 2009: pp. 1–6.

[29]   A.M. Divakaran, D. Hamilton, K.N. Manjunatha, M. Minakshi, Design, Development and Thermal Analysis of Reusable Li-Ion Battery Module for Future Mobile and Stationary Applications, Energies. 13 (2020) 1477. https://doi.org/10.3390/en13061477.

[30]   S. Barcellona, L. Piegari, Lithium Ion Battery Models and Parameter Identification Techniques, Energies. 10 (2017) 2007. https://doi.org/10.3390/en10122007.

[31]   Casals, Rodríguez, Corchero, Carrillo, Evaluation of the End-of-Life of Electric Vehicle Batteries According to the State-of-Health, World Electric Vehicle Journal. 10 (2019) 63. https://doi.org/10.3390/wevj10040063.

[32]   S. Buller, M. Thele, R.W.A.A. DeDoncker, E. Karden, Impedance-Based Simulation Models of Supercapacitors and Li-Ion Batteries for Power Electronic Applications, IEEE Transactions on Industry Applications. 41 (2005) 742–747. https://doi.org/10.1109/TIA.2005.847280.

[33]   W. Waag, S. Käbitz, D.U. Sauer, Experimental investigation of the lithium-ion battery impedance characteristic at various conditions and aging states and its influence on the application, Applied Energy. 102 (2013) 885–897. https://doi.org/10.1016/j.apenergy.2012.09.030.

[34]   M. Uno, K. Tanaka, Influence of High-Frequency Charge–Discharge Cycling Induced by Cell Voltage Equalizers on the Life Performance of Lithium-Ion Cells, IEEE Transactions on Vehicular Technology. 60 (2011) 1505–1515. https://doi.org/10.1109/TVT.2011.2127500.

[35]   M. Minakshi, D.R.G. Mitchell, A.R. Munnangi, A.J. Barlow, M. Fichtner, New insights into the electrochemistry of magnesium molybdate hierarchical architectures for high performance sodium devices, Nanoscale. 10 (2018) 13277–13288. https://doi.org/10.1039/C8NR03824D.

[36]   N. Al-Zubaidi R-Smith, M. Leitner, I. Alic, D. Toth, M. Kasper, M. Romio, Y. Surace, M. Jahn, F. Kienberger, A. Ebner, G. Gramse, Assessment of lithium ion battery ageing by combined impedance spectroscopy, functional microscopy and finite element modelling, Journal of Power Sources. 512 (2021) 230459. https://doi.org/10.1016/j.jpowsour.2021.230459.

[37]   J.P. Pender, G. Jha, D.H. Youn, J.M. Ziegler, I. Andoni, E.J. Choi, A. Heller, B.S. Dunn, P.S. Weiss, R.M. Penner, C.B. Mullins, Electrode Degradation in Lithium-Ion Batteries, ACS Nano. 14 (2020) 1243–1295. https://doi.org/10.1021/acsnano.9b04365.

[38]   L. Wang, B. Chen, J. Ma, G. Cui, L. Chen, Reviving lithium cobalt oxide-based lithium secondary batteries-toward a higher energy density, Chemical Society Reviews. 47 (2018) 6505–6602. https://doi.org/10.1039/C8CS00322J.